Journal of the Australian Ceramic Society (2022) 58:1509–1517
https://doi.org/10.1007/s41779-022-00789-0

RESEARCH

# Preparing weathering-resistant superhydrophobic polymer/bentonite nano-composites for waterproof garment textiles via electrospinning

**Die Hu**[1]

Received: 27 April 2022 / Revised: 24 July 2022 / Accepted: 9 August 2022 / Published online: 19 August 2022


## Abstract

Polymers can be prepared into textiles via electrospinning. However, high overall property of outdoor clothing is necessary. In this work, hybridization and electrospinning were employed to fabricate fluoropolymer@bentonite hybrid textiles. Compared with fluoropolymer textile, hybrid textiles exhibit a surface superhydrophobicity ascribed to the significantly improved surface roughness of hybrid fibers, and they display high thermal stability attributed to inorganic bentonite. After acid/alkali immersion, ultraviolet radiation, or mechanical abrasion, hybrid textiles still show high water resistance, indicating strong weathering resistance. Rational material selection and electrospinning result in low surface energy, high surface roughness, and binary micro/nano hierarchical structure. Hybrid textile (with 10 wt% bentonite) shows high overall property (water contact angle of ~ 155°; thermal stability up to ~ 400 ℃; superhydrophobicity after 48 h exposing to acid, alkali, or radiation; hydrophobicity after 100 abrasion cycles). This work might pave a road for large-scale preparation of high-performance textiles for waterproof garments.

**Keywords** Electrospinning · Superhydrophobic · Nano-composite · Bentonite · Weather-resistant

## Introduction

Practicability, comfort, economy, and esthetic are considered when clothing materials are studied [1]. Advantages of clothing materials should include structural stability, mechanical strength, flexibility, breathability, and light-weight feature [2]. Outdoor suits should show good waterproofness and weathering resistance (thermotolerance, acid/alkali resistance, ultraviolet (UV) resistance, and abrasion resistance) [3]. Polymeric fibers are good candidates for fabricating garment fabrics [4]. Chemical fiber fabrics are made from polyethylene terephthalate, polyamide, and polyacrylonitrile [5]. They can show some advantages (wear-resistant; not moldy) [6]. Material processing is essential to macroscopical properties of garment fabrics. Electrospinning plays a key role in preparing fiber textiles (the ordered or complex components) [7]. For high-performance outdoor fabrics, the selection and processing of materials are vital.

The lotus-leaf bionic superhydrophobic trait of the surfaces of outdoor fabrics has been desirable in clothing industry [8]. Based on substantial research on superhydrophobic surfaces, both of low surface energy (relying on surface elemental composition) and high surface roughness (relying on binary micro/nano hierarchical structure) are compulsory [9]. Polymeric fibers have been confirmed to be leading candidates for preparing garment fabrics. The low-roughness surfaces consisting of water-repellent fluoropolymers cannot show a superhydrophobicity but a hydrophobicity [10]. Using fluoropolymers, the surfaces cannot obtain a superhydrophobicity in most cases. Therefore, the hybrid strategy has been adopted to fabricate fluoropolymer/particles hybrid surfaces for achieving superhydrophobicity [11].

With respect to material selection, the polyvinylidene fluoride (PVDF) with ultra-low surface energy from F element [12] and the bentonite (BT) particles with lamellar morphology and low surface friction coefficient [13] can be promising. In detail, PVDF is hydrophobic and semi-crystalline [14], and it can possess outstanding piezoelectricity, chemical resistance, thermal stability, hydrophobic stability, mechanical property, and film-forming property

✉ Die Hu
hudie202224@163.com

[1] School of Fashion Engineering, Jiangxi Institute of Fashion Technology, No. 103, Lihuzhong Avenue, Xiangtang Economic Development Zone, Nanchang 330201, People's Republic of China

[15]. Compared with the other commercialized hydrophobic polymers such as fluorinated copolymers, easy synthesis of PVDF (simple homopolymer) for a low cost can be followed [16]. In detail, BT material can have 2:1 layered silicate structure (bearing silicon-oxygen tetrahedrons and aluminum-oxygen octahedrons) [17]. BT can show several advantages such as low cost (traditional and easily available nonmetallic ore), high stability, and easy dispersibility (large specific surface area and interlayer structure) [18]. Compared with the other materials used in the same context (such as carbide particles), abundant -OH groups at the surface of BT can provide a possibility of introducing novel active functional groups and improving BT/matrix interface compatibility (high dispersibility of BT) [19].

To realize superhydrophobicity and high weathering resistance, in this work, the PVDF@BT hybrid fiber textiles have been prepared via electrospinning. Employing high-efficiency electrospinning can favor the hybrid fibers to achieve an ultrahigh aspect ratio. First, the BT suspension containing the dissolved PVDF was electrospun to form the hybrid fiber textiles. Then, the overall property (static water contact angle, thermotolerance, and weathering resistance under various factors of damage) of hybrid textiles was studied. In the end, a superior overall property of hybrid fiber textiles to neat PVDF fiber textile was clarified based on several factors (surface energy, surface roughness, and binary micro/nano hierarchical structure). The hybrid fiber textile with 10 wt% BT can show a high overall property (water contact angle of ~ 155°; thermal stability up to ~ 400 ℃; superhydrophobicity after 48 h exposing to acid, alkali, or ultraviolet radiation; good hydrophobicity after 100 abrasion cycles). The innovation of this work should lie in an excellent synergy between high-aspect-ratio PVDF fibers and lamellar BT particles in hybrid fiber textiles. This work might pave a road for a large-scale preparation of the high-performance textiles applicable in the advanced long-life waterproof garments.

## Experimental

### Materials

Polyvinylidene fluoride (PVDF, 99.9%, AR grade, $M_w$ ~ 100 kDa) powder was purchased from Alfa Aesar (Tianjin, China). Bentonite (BT, AR grade) powder was purchased from Aladdin. N,N-dimethylformamide (DMF, 99.5%, AR grade) was obtained from Zibo Nature International Trading Co., Ltd. (Zibo, China). All the materials were used as received, without any pretreatment.

### Preparation of PVDF@BT hybrid textiles

Here, the film-shaped PVDF@BT hybrid textiles were fabricated by electrospinning process [20]. In the resultant hybrid textiles, the mass fractions of BT component were designed to be 0 wt%, 1 wt%, 2 wt%, 5 wt%, and 10 wt%, respectively. Firstly, PVDF powder and BT powder with the designed feed ratio (PVDF 1.5 g and BT 0–0.15 g) were added into DMF of 10 mL. Later, a fierce magnetic stir to the mixture was performed at 120 ℃ for 2 h, leading to a formation of the even particle-suspension. At last, the particle-suspension was transferred into an injector (the volume of 20 mL) followed by carrying out electrospinning over time at 25 ℃ (process conditions: special syringe needle with pinhole diameter of 1.25 mm; operating at 15 kV; adopting the plate-type receiving device covered with aluminum foil; the distance between needle head and receiving plate was 15 cm; spinning speed of 1.00 mL/h) to yield the PVDF@BT hybrid fiber cloth (quadrate; the area up to 30 × 50 cm; the thickness can be controlled by electrospinning time).

In Fig. 1, the schematic diagram for showing the fabrication route of hybrid textiles was given.

### Characterization

X-ray diffraction (XRD) data were obtained based on a Rigaku D/max 2400 diffractometer (Japan) with X-ray wavelength of 1.542 Å (Cu Kα radiation; 40 kV; 100 mA), scanning speed of 5°/min, and scanning step of 0.02°. Proton nuclear magnetic resonance ($^1$H NMR) data were achieved based on a Bruker (Advance III) 400 MHz spectrometer (taking acetone-$d_6$ as the solvent and tetramethylsilane as the inner standard). Field-emission scan electron microscopy (FE-SEM) images were obtained from a ZEISS EVO18 (Germany) at 5 kV. Transmission electron microscopy (TEM) images were collected from a JEM-200CX with 200 kV. The static contact angle (CA) data were obtained

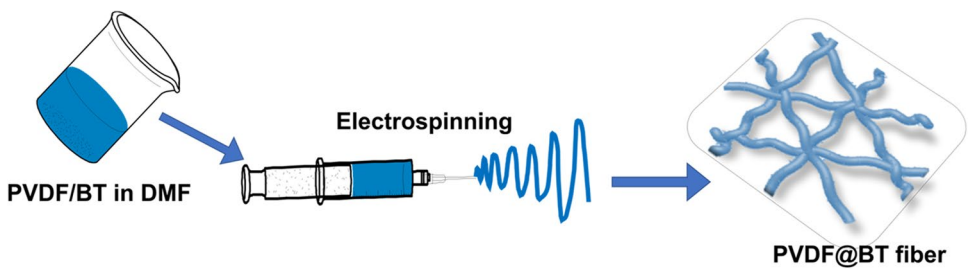


**Fig. 1** Schematic diagram to show the fabrication route of hybrid textiles

based on a dynamic static state surface contact angle instrument (PG-X) (the volume of the deionized water droplet was ~ 5 μL). Thermogravimetric analysis (TGA) was executed on a NJKHTG-1. The surface abrasion treatments (with various abrasion cycles; using a sandpaper) were performed based on the "paint/double-sided tape"-treated glass [10]. Fourier-transform infrared (FT-IR) spectra were recorded on an IR spectrophotometer (Bruker-Tensor 27). The pore-size distribution results were collected from a pore size analyzer PMI CFP-1100Al (Porous Materials Inc.).

## Results and discussion

### Characterization of original materials

To verify the crystal form of BT, its XRD curve is shown in Fig. 2a. Based on diffraction peaks, bentonite can be verified to have the chemical formula of $Al_2O_3{\cdot}4(SiO_2){\cdot}H_2O$ and show a dioctahedral smectite structure (layered structure; lamellar crystal; silicate clay ore; monoclinic system) [21]. To confirm the chemical composition of PVDF, its $^1$H NMR spectrum is displayed in Fig. 2b. The peaks at 2.2–2.7 ppm and 2.7–3.2 ppm should be respectively attributed to the head-head (-$CF_2$-C$H_2$-C$H_2$-$CF_2$-) and head–tail (-$CF_2$-C$H_2$-$CF_2$-C$H_2$-) connections of VDF structural units in PVDF [22]. The peaks from solvent and inner standard are found as well. The chemical composition of PVDF can be confirmed to contain 90 mol% of head–tail connection and 10 mol% of head-head connection (VDF structural units) based on areal integrals.

To confirm the micro-morphology of BT particles, SEM and TEM images of them are presented in Fig. 3a and b, respectively. According to SEM result, the particle sizes of BT particles can be found to vary between 200 and 800 nm, and the average particle size of them can be verified to be 500 nm. The lamellar two-dimensional morphology of BT particles can be confirmed. Based on TEM result (see gray-level), the lamellar trait of BT particles is further verified.

### Crystalline property and surface morphology of PVDF@BT textiles

To confirm the crystallization capacity of PVDF@BT hybrid textiles, the XRD result of PVDF@BT hybrid (with 10 wt% BT, the representative sample) is given in Fig. 4. For comparison, the XRD result of neat BT sample is exhibited again in the figure. Differing from a strong crystalline capacity of neat BT material discussed above, the hybrid is found to

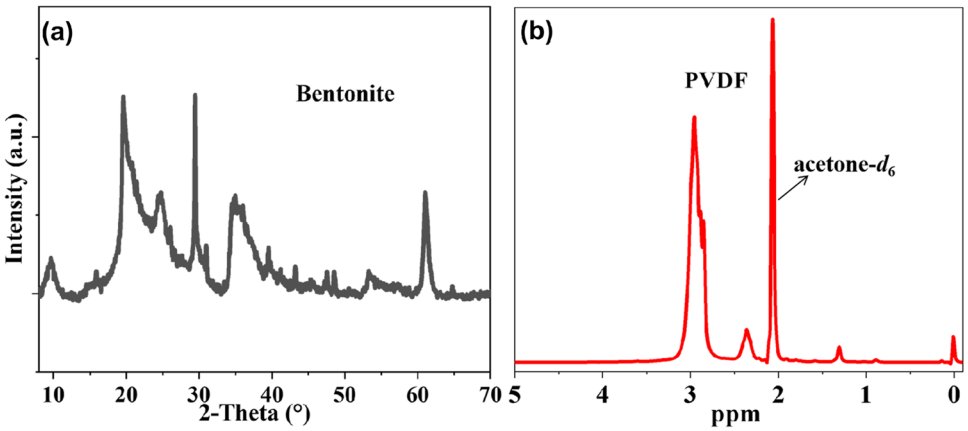


**Fig. 2** **a** XRD curve of BT and **b** $^1$H NMR spectrum of PVDF

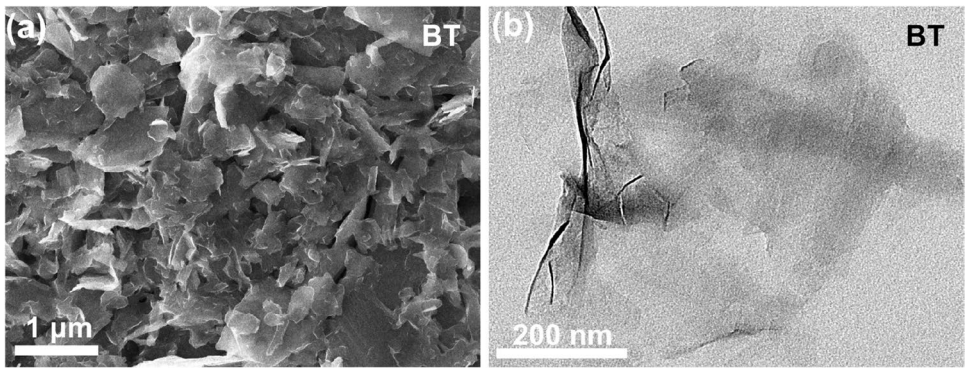


**Fig. 3** **a** SEM and **b** TEM images of BT sample

show a weak crystalline capacity based on the blunt wide peak (between 10° and 40°). This wide peak can suggest the predominant beta crystalline phase in the electrospun PVDF component in PVDF@BT hybrid [23]. Because of the relatively low content for BT particles in the hybrid, the high-intensity sharp peaks of BT component in the hybrid have been covered. Moreover, the surface transfer of PVDF can lead to the efficient coating of PVDF to BT surfaces, further resulting in the covered BT signals. In a word, PVDF@BT hybrid can show the notably reduced crystallization capacity compared with neat BT material. In Fig. S1, the XRD results of all hybrids (different BT contents) can be achieved.

Now, the surface micro-morphology of PVDF@BT hybrid textiles should be researched. First, the SEM images of neat PVDF textile (PVDF@BT hybrid with 0 wt% BT) are displayed in Fig. 5. In Fig. 5a, the low-magnification SEM image of pure PVDF textile is shown. The relatively uniform size distribution of PVDF fibers in the textile can be observed. In terms of the applications of clothing materials (the strong structural stability and good permeability/perspiration traits), the favorable interpenetrating network structure and porous structure in neat PVDF textile can be verified [24]. The threadlike one-dimensional feature of each PVDF fiber in the textile film can be justified ascribed to the employed electrospinning technology [25]. The electrospinning can serve a large-scale fabrication of various fibers. In the present case, the PVDF solution (high-polarity DMF as solvent) can be sprayed under a high external electric field. Driven by the electric field, the droplets at the tip of needle can change from sphericity to "Taylor cone" [26], and then they can extend from the tip of the "Taylor cone" to form PVDF fiber filaments. Furthermore, in Fig. 5b, the locally amplified SEM image of neat PVDF textile is achieved. The observed PVDF fiber with a high uniformity can show a diameter of ~ 800 nm. Owing to the single-component trait, the surface of the observed fiber is relatively smooth. In the end, in Fig. 5c, the high-magnification SEM result of neat PVDF textile is provided. The surface roughness should stem from the fine crystalline grains of PVDF fiber surface [27].

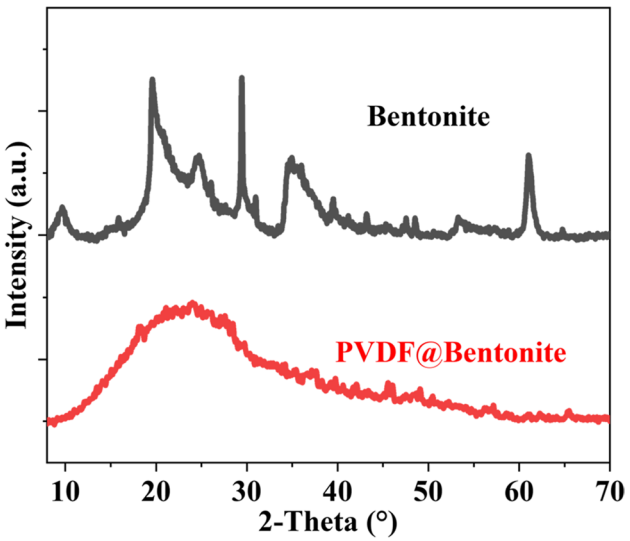


**Fig. 4** XRD result of PVDF@BT hybrid with 10 wt% of BT

In Fig. 6, the SEM images of PVDF@BT hybrid textile with 10 wt% BT are presented. Based on low-magnification SEM result in Fig. 6(a), the homogeneous distribution of diameters of those hybrid fibers can be confirmed, and the woven morphology (the interpenetrating networks and the pores) of sample can be verified as well. Those hybrid fibers can have huge length-diameter ratios. The inset of Fig. 6a exhibits the photo of film-like material object. Moreover, the further amplified SEM result of hybrid textile is exhibited in Fig. 6b. For dress fabric, the observed micro-structure here is favorable. Furthermore, in Fig. 6c, the SEM image of the sample for observing more details is provided. The electrospinning can guarantee the homogeneity in diameters (~ 800 nm) of hybrid fibers with BT particles. In comparison with neat PVDF fibers discussed above, PVDF@BT hybrid fibers can exhibit a significantly improved surface roughness, ascribed to the lamellar granular trait of BT [28] as well as the migration of partial F atoms of PVDF component towards the surface of hybrid fibers (decreasing surface energy) [29]. At last, the high-amplification SEM image of hybrid fiber is shown in Fig. 6d. The high surface roughness of hybrid fiber can be observed. Compared with neat BT particles, the BT particles at the surface of PVDF@BT hybrid fiber can be well encapsulated by PVDF component

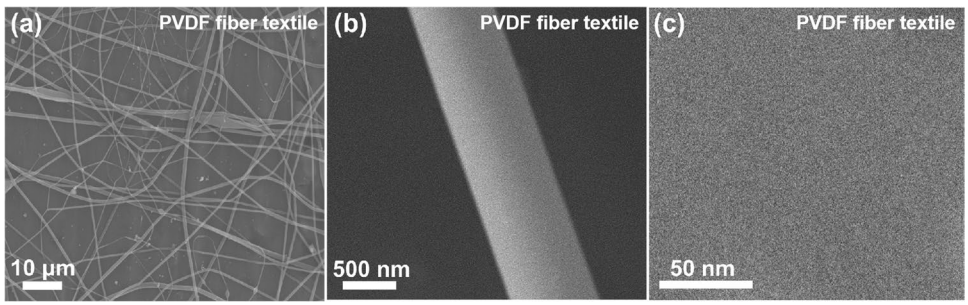


**Fig. 5** SEM images of neat PVDF fiber textile with various magnification. **a** Low-magnification, **b** middle-magnification and **c** high-magnification SEM images of PVDF fiber textile without bearing BT

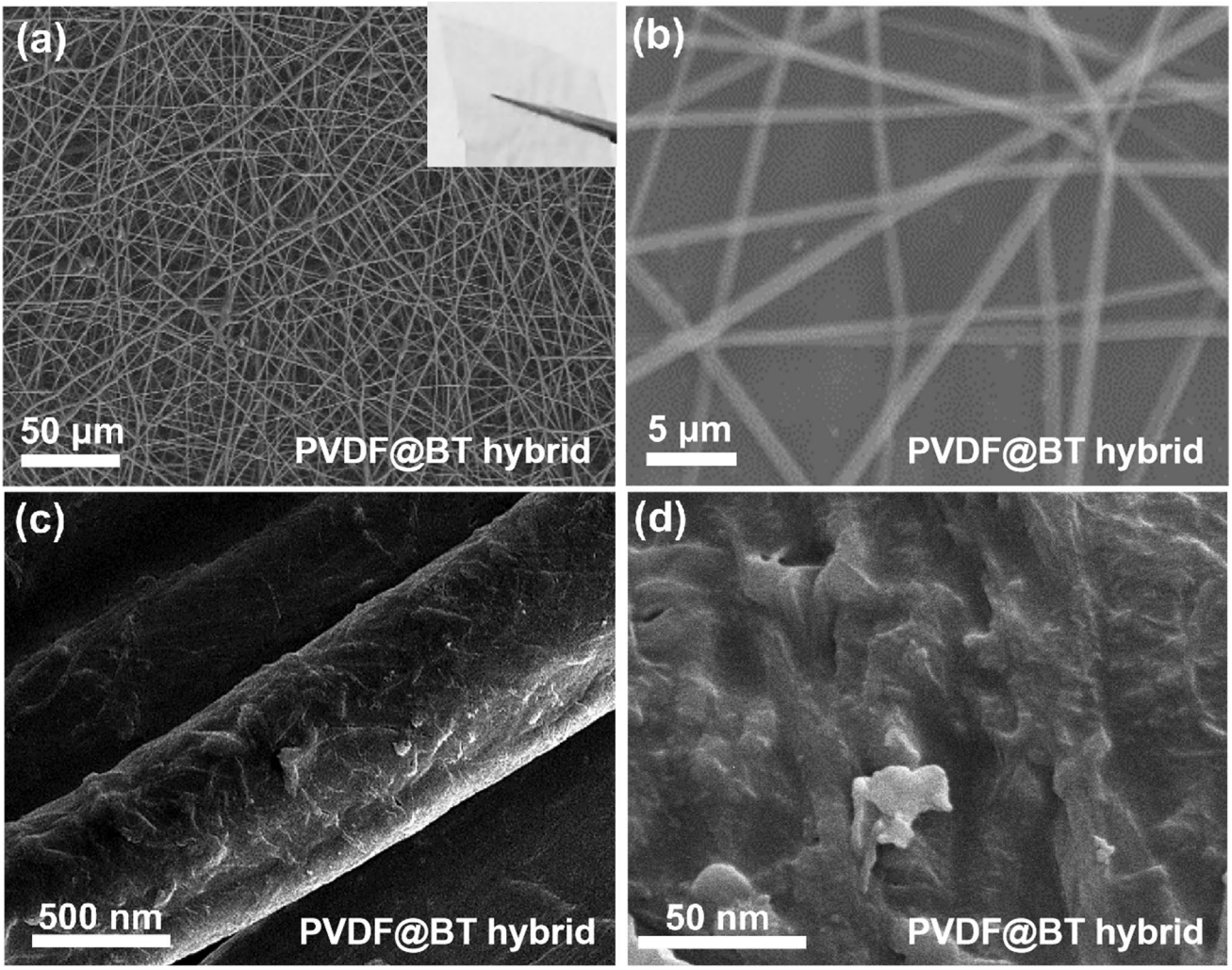


**Fig. 6** SEM images of PVDF@BT hybrid with 10 wt% BT with various amplification. **a** Low-magnification SEM image (the inset for film photo), **b** further amplified SEM image, **c** middle-magnification SEM image, and **d** high-magnification SEM image of PVDF@BT hybrid with 10 wt% BT

based on the present image. This can be explained by the fact that the electrospinning has been performed to the uniform mixture of PVDF and BT materials in DMF. The SEM image of hybrid fibers with 20 wt% BT is given in Supporting Information (Fig. S2). More SEM images are given in Fig. S3, and the optimal BT content can be confirmed as 10 wt%. In Fig. S4, FT-IR spectra of pristine PVDF fibers and PVDF@BT hybrid fibers (10 wt% BT) are given, and the pore-diameter distribution diagrams of two samples are also given.

## Water repellency and thermotolerance of PVDF@BT hybrids

Usually, outdoor clothing materials are required to show a high water repellency and thermotolerance [30]. Herein, the water repellency and thermotolerance of the as-prepared PVDF@BT hybrid textiles are researched. In Fig. 7a, the static water contact angles of the surfaces of PVDF@BT hybrid textiles with various BT contents are achieved. The neat PVDF fiber textile is measured to have a contact angle of ~ 110.7 ± 2 degrees (hydrophobic), attributed to the massive F atoms (ultra-low surface energy) at the surfaces of neat PVDF fibers [31] as well as the porous structure (holding air mattress) at the surface of the whole textile [32]. The SEM result in Fig. 5a can verify the porous structure at the surface of neat PVDF fiber textile. When the BT content in hybrid increases, the water contact angle of the surface of hybrid fiber textile can be increased. From 0 to 2 wt% (BT content), the contact angle of sample surface is quickly improved ascribed to the notably increased surface roughness of hybrid fiber textile from the addition of lamellar

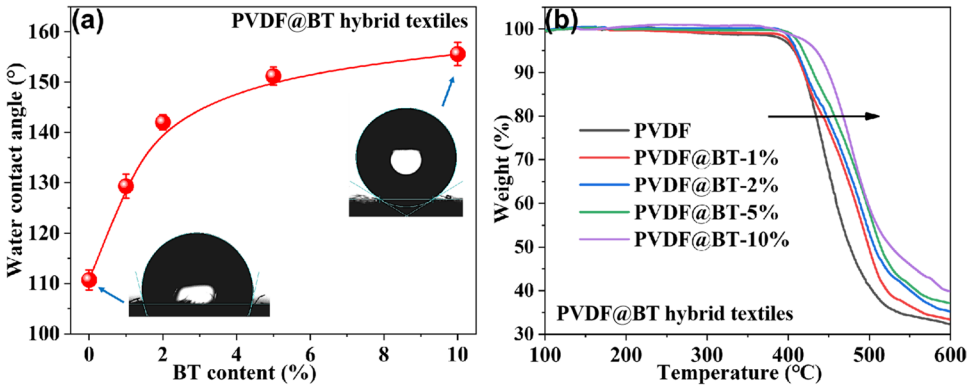


**Fig. 7** **a** Water contact angles and **b** TGA results of PVDF@BT hybrid textiles

BT particles [33]. From 2 to 10 wt% (BT content), the contact angle of sample surface is slowly elevated attributed to the slowly increased surface roughness of textile (possibly approaching a saturation of surface roughness at 10 wt%) [34]. At 5 wt% and 10 wt% (BT contents), the superhydrophobic properties (> 150 degrees) of two surfaces in hybrid fiber textiles can be confirmed [35].

Differing from neat PVDF fibers with low surface energy and low surface roughness (see Fig. 5c), PVDF@BT hybrid fibers can possess both of the low surface energy and high surface roughness (referring to Fig. 6d), which can clarify the superhydrophobicity of the two surfaces in hybrid textiles aforementioned [36]. In detail, the partial F element (ultra-low surface energy) in PVDF can spontaneously migrate to the surface of PVDF@BT hybrid fibers (a good coating of PVDF to the surfaces of BT particles in Fig. 6d), which can result in a favorable low surface energy of hybrid fibers for strong water repellency. More importantly, the well-coated lamellar BT particles (neat BT particles with some flexibility; see Fig. 3a) at the surfaces of hybrid fibers can lead to a favorable high surface roughness of hybrid fibers for strong water repellency as well. In fact, hybrid fiber textiles (see Fig. 6a) should consist of hybrid fibers (forming the interpenetrating networks) and massive air mattresses (in the micro-pores), indicating a favorable binary micro/nano hierarchical structure [37] at the entire surface of hybrid fiber textile. This hierarchical surface structure is very helpful to achieving a superhydrophobicity at textile surface. To sum up, the introduction of BT particles and the electrospinning of hybrid are of great importance, for a superhydrophobicity. In Fig. 7a, the microscopic photos of the two samples (0 wt% and 10 wt%) during the tests of contact angles are given in the insets. When BT content is 10 wt%, the highest static water contact angle of textile surface can reach ~ 155.6 ± 2.3 degrees.

In Fig. 7b, TGA results of all hybrid fiber textiles are displayed. While the temperature is improved from 100 to 400 ℃, the extremely slow decrease of the weight of all the samples can be found due to the evaporation of the adsorbed impurities with the extremely low contents as well as the removal of crystal water in crystalline BT component [38]. From 400 to 600 ℃, a rapid decrease of the weight of all samples can be confirmed owing to a quick degradation of macromolecular chains in PVDF component (organic nature) [39]. Moreover, in the range of 400–600 ℃, the hybrid fiber textile with more BT particles (compared with the textile with fewer particles) can show the same weight loss (in percentage) at a higher temperature, which can be due to a far higher decomposition temperature of inorganic BT component than organic PVDF component [40].

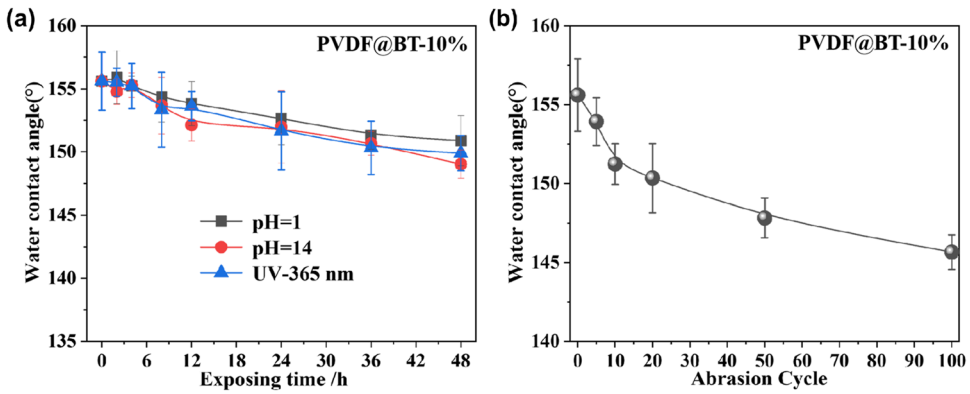


**Fig. 8** **a** Water contact angles of the surface as a function of exposing time to various harmful factors, and **b** water contact angles of the surface after various abrasion cycles

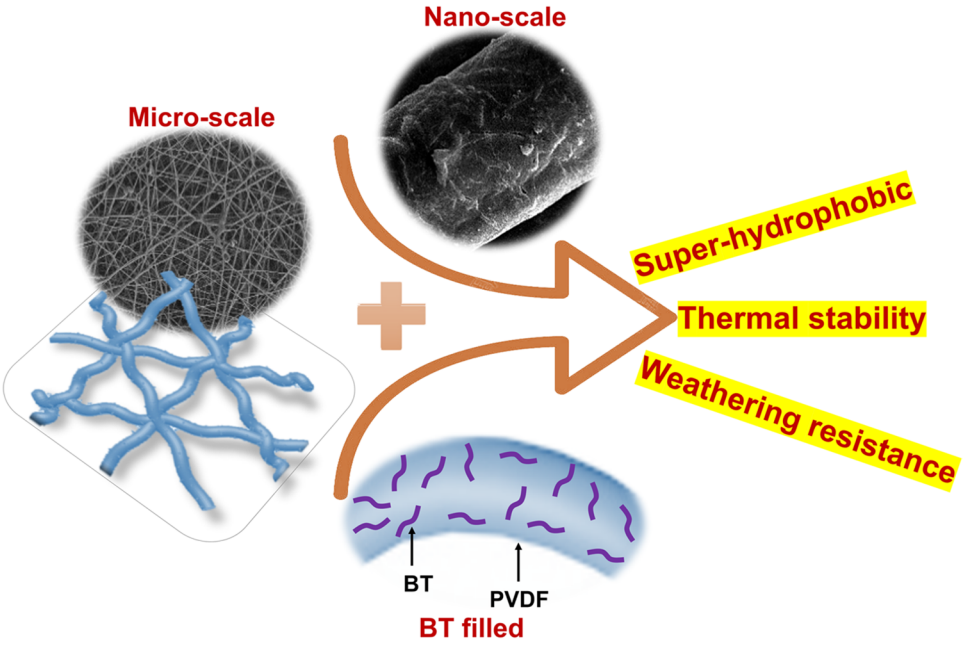


**Fig. 9** Schematic diagram to exhibit the micro-mechanism of good comprehensive property in hybrid textiles

Compared with pure PVDF fiber textile, those PVDF@BT hybrid fiber textiles can exhibit the improved high thermotolerance for clothing applications, indicating the advantage of organic–inorganic hybrid fibers [41]. To sum up, in the light of water resistance and thermotolerance, PVDF@BT hybrid fiber textiles are more promising than neat PVDF fiber textile in practical applications of outdoor clothes.

## Weathering resistance of the representative PVDF@BT textile

Actually, the state-of-the-art outdoor clothing fabrics are often required to exhibit a strong weathering resistance (considering acid corrosion, alkaline corrosion, ultraviolet radiation, and surface abrasion) [42]. Here, the weathering resistance of the representative PVDF@BT hybrid fiber textile (with 10 wt% BT) is investigated via the change of static water contact angle of the surface of this textile under various external environments. In Fig. 8a, the water contact angles of sample surface are achieved as a function of the exposing time to various external environments (pH = 1, pH = 14 and 365 nm ultraviolet (UV) radiation, respectively). The original contact angle of the surface can reach ~ 155.6 ± 2.3 degrees to mean a superhydrophobicity. When the exposing time is increased from 0 to 48 h, the contact angle of the surface which is exposed to strong acid, base, or UV-radiation can be found to slowly reduce to generally maintain a superhydrophobicity. That can suggest a robust acid-resistance, alkali resistance and UV resistance (a good weathering resistance) of textile surface. Based on superhydrophobicity of the initial surface, either the acidic substance or the alkaline substance dissolved in the water cannot strongly corrode the soaked textile [43], which can explain the robust acid/alkali resistances of textile surface discussed above. Furthermore, the ultrahigh C-F bond strength in PVDF component should be responsible for robust UV resistance of hybrid textile analyzed above [44].

In Fig. 8b, the water contact angles of textile surface after various abrasion cycles are obtained. The initial surface (abrasion cycle = 0) can display the highest water contact angle. With an increase of abrasion cycle number from 0 to 100, the contact angle of textile surface can be gradually reduced. After 100 abrasion cycles, a high water contact angle of ~ 145.6 ± 1.1 degrees (strong water repellency) can still be maintained at surface, which should stem from a loose micro-structure (containing lots of air mattresses; buffering to absorb the energy) of PVDF@BT hybrid fiber textile as well as the layered micro-structure of BT particles with a low surface friction coefficient (a strong lubricity). To sum up, the as-prepared PVDF@BT hybrid fiber textiles can possess a strong weathering resistance for applications in outdoor clothing fabrics, and meanwhile, a high structural stability of PVDF@BT hybrid fibers (based on well-maintained surface hydrophobicity) can be confirmed.

In Fig. 9, the schematic diagram to exhibit the micro-mechanism of a good comprehensive property of PVDF@BT hybrid fiber textiles is provided. In addition to F element at the surface of hybrid fibers, the high micro-scale surface roughness of textiles and the high nano-scale surface roughness of hybrid fibers can jointly contribute to superhydrophobic properties of textile surfaces. Moreover, filling BT into PVDF matrix compared with neat PVDF textile can lead to high thermal stability of hybrid textiles. Finally, the high weathering resistance of hybrid textiles should be attributed

to the rationally selected ingredients and the electrospinning-induced favorable micro-morphology.

## Conclusion

In this work, the highly waterproof PVDF@BT hybrid fiber textiles applicable for weathering-resistant outdoor clothing fabrics have been fabricated through electrospinning of particle suspension. The PVDF@BT hybrid fiber textiles can show a strong surface hydrophobicity (superhydrophobicity at the high BT contents), and the hybrid fiber textiles have a remarkably improved water repellency compared with neat PVDF fiber textile. Both of the low surface energy (F element from PVDF component) and high surface roughness (from lamellar BT particles) should be responsible for the superhydrophobicity achieved at the surfaces of hybrid fiber textiles. The electrospinning can induce a formation of the favorable micro-structure of hybrid textiles consisting of the interpenetrating networks (hybrid fibers with an ultrahigh aspect ratio) and abundant tiny air mattresses (in the micro-pores), suggesting a formation of binary micro/nano hierarchical structure at the surfaces of PVDF@BT hybrid fiber textiles. The hybrid fiber textiles are found to show a higher thermal stability than neat PVDF fiber textile, ascribed to inorganic BT component. The high weathering resistance of hybrid textiles has been verified based on good maintenance of surface water contact angle (damage factors: acid, alkali, UV radiation, and mechanical abrasion). As a result, the PVDF@BT hybrid textile (with 10 wt% BT) can exhibit a promising overall property (static water contact angle of ~ 155.6 ± 2.3 degrees; heat-resistant upper limit of ~ 400 ℃; superhydrophobicity maintenance after 48 h of the exposing to acid, alkali, or UV radiation; strong hydrophobicity after 100 abrasion cycles) for outdoor clothing applications. This work might open up a way for a large-scale preparation of the organic–inorganic hybrid fiber textiles with a high overall property for the applications in modern waterproof garments.

**Supplementary Information** The online version contains supplementary material available at https://doi.org/10.1007/s41779-022-00789-0.

**Funding** This work was supported by the Science and Technology Project of Education Department of Jiangxi Province (grant numbers GJJ202405; GJJ191087; GJJ202412).

**Data availability** The datasets generated during and/or analyzed during the current study are available from the corresponding author on reasonable request.

## Declarations

**Conflict of interest** The author declares no competing interests.

## References

1. Bartkowiak, G., Marszałek, A., Dąbrowska, A: Materials **13**, 4320 (2020)
2. Bhattacharjee, S., Joshi, R., Chughtai, A.A., Macintyre, C.R.: Adv. Mater. Interfaces **6**, 1900622 (2019)
3. Gibson, G.: J. Ind. Text. **38**, 43 (2008)
4. Gao, Y.-N., Wang, Y., Yue, T.-N., Weng, Y.-X., Wang, M.: J. Colloid Interface Sci. **582**, 112 (2021)
5. Hwang, S.-H., Kim, Y.K., Jeong, S.M., Choi, C., Son, K.Y., Lee, S.-K., Lim, S.K.: Text. Res. J. **90**, 2198 (2020)
6. Feng, Z., Hu, F., Lv, L., Gao, L., Lu, H.: RSC Adv. **11**, 25530 (2021)
7. Canejo, J.P., Borges, J.P., Godinho, M.H., Brogueira, P., Teixeira, P.I.C., Terentjev, E.M.: Adv. Mater. **20**, 4821 (2008)
8. Altay, P., Atakan, R., Özcan, G.: Fibers Polym. **22**, 1025 (2021)
9. Li, M., Luo, W., Sun, H., Xu, J., Ng, K.W., Cheng, X.: ACS Appl. Nano Mater. **4**, 12300 (2021)
10. Feng, Y., Peng, C., Hu, J., Wang, F., Xu, Z., Huang, Q.: J. Mater. Chem. A **6**, 14262 (2018)
11. Xin, Q., Li, X., Hou, H., Liang, Q., Guo, J., Wang, S., Zhang, L., Lin, L., Ye, H., Zhang, Y.: ACS Appl. Mater. Interfaces **13**, 1827 (2021)
12. Hardman, S.J., Muhamad-Sarih, N., Riggs, H.J., Thompson, R.L., Rigby, J., Bergius, W.N.A., Hutchings, L.R.: Macromolecules **44**, 6461 (2011)
13. Demets, G.J.F., Anaissi, F.J., Toma, H.E., Fontes, M.B.A.: Mater. Res. Bull. **37**, 683 (2002)
14. Fontananova, E., Bahattab, M.A., Aljlil, S.A., Alowairdy, M., Rinaldi, G., Vuono, D., Nagy, J.B., Drioli, E., Di Profio, G.: RSC Adv. **5**, 56219 (2015)
15. Rui, G., Allahyarov, E., Li, R., Taylor, P.L., Zhu, L.: Mater. Horiz. **9**, 1992 (2022)
16. Shah, A.A., Heo, H.J., Park, S., Yi, E., Cho, Y., Nam, S.-E., Park, Y.-I., Kim, H., Sohn, E.-H., Park, H., Kim, J.F.: ACS Appl. Polym. Mater. **2**, 5249 (2020)
17. Can, H.K., Sevim, H., Şahin, Ö., Gürpınar, Ö.A.: Polym. Bull. **79**, 5549 (2022)
18. Patro, T.U., Mhalgi, M.V., Khakhar, D.V., Misra, A.: Polymer **49**, 3486 (2008)
19. Wireko, C., Abichou, T.: Geotext. Geomembr. **49**, 1004 (2021)
20. Qu, L., Zhang, W., Zhao, G., Zhao, D.: Ceram. Int. **47**, 15114 (2021)
21. Šucha, V., Uhlík, P., Madejová, J., Petit, S., Kraus, I., Puškelová, L.: Clay. Clay Miner. **55**, 36 (2007)
22. Feng, Y., Wu, Q., Deng, Q., Peng, C., Hu, J., Xu, Z.: J. Mater. Chem. C **7**, 6744 (2019)
23. Baji, A., Mai, Y.-W., Abtahi, M., Wong, S.-C., Liu, Y., Li, Q.: Compos. Sci. Technol. **88**, 1 (2013)
24. Fan, X., Wang, X., Yan, H., Cai, M., Zhong, W., Li, H., Zhu, M.: Colloids Surf. A: Physicochem. Eng. Asp. **639**, 128323 (2022)
25. Yang, G., Wang, L., Wang, J., Yan, W.: Ceram. Int. **43**, 71 (2017)
26. He, J.-H.: Results Phys. **17**, 103096 (2020)
27. Zhang, X.-Y., Zhang, X.-Y., Guo, S.-R.: J. Sulfur Chem. **32**, 23 (2011)
28. Ma, J., Li, D., Zhang, W., Lei, C.: J. Chem. Technol. Biotechnol. **85**, 288 (2010)
29. Li, W., Zou, Y.-Q.: Chin. J. Polym. Sci. **32**, 1032 (2014)
30. Erayman Yüksel, Y., Korkmaz, Y.: Int. J. Cloth. Sci. Technol. **31**, 693 (2019)
31. Chen, T.-B., Li, Q.-N., Liu, C., Hong, R., Li, Q., Zhu, L., Xu, C.: Chem. Eng. J. **411**, 128623 (2021)
32. Wu, Q., Liu, C., Gong, J., Wang, Y., Liu, D., Meng, Q., Mao, H., Geng, X., Song, X.-M.: Appl. Surf. Sci. **570**, 151202 (2021)

33. Yu, L., Kang, Y., Tang, H., Zhou, J.: ACS Appl. Mater. Interfaces **11**, 7510 (2019)
34. Forgerini, F.L., Figueiredo, W.: Phys. Rev. E **79**, 041602 (2009)
35. Patel, S.U., Manzo, G.M., Patel, S.U., Kulkarni, P.S., Chase, G.G.: J. Nanotechnol. **2012**, 483976 (2012)
36. Niu, B., Yang, S., Hua, T., Tian, X., Koo, M.: Nano Res. **14**, 1043 (2021)
37. Wei, Y., Hu, Y., Li, M., Li, D.: J. Bionic Eng. **17**, 1186 (2020)
38. Yaghoubi, Z., Basiri-Parsa, J.: J. Water Process Eng. **34**, 101067 (2020)
39. Silva, R.A., Silva, P.A., Carvalho, M.E.: Mater. Sci. Forum **539–543**, 573 (2007)
40. Arroyo, M., Suárez, R.V., López-Manchado, M.A., Fernández, J.F.: J. Nanosci. Nanotechnol. **6**, 2151 (2006)
41. Ghosh, P., Naskar, K., Das, N.C.: Compos. Part C: Open Access **2**, 100018 (2020)
42. Qin, H., Li, X., Zhang, X., Guo, Z.: New J. Chem. **43**, 5839 (2019)
43. Feng, Y., Peng, C., Li, Y., Hu, J., Deng, Q., Wu, Q., Xu, Z.: J. Colloid Interface Sci. **536**, 149 (2019)
44. Liu, Z., Zhang, C., Zhang, X., Wang, C., Liu, F., Yuan, R., Wang, H.: Chem. Eng. J. **411**, 128632 (2021)